Performance of historical ferrocement specimens subjected to corrosive environments

(Article begins on next page)

14 March 2025

fib WILEY

Performance of historical ferrocement specimens subjected to corrosive environments

Erica Lenticchia [ID] | **Gerardo Sorrentino** | **Rosario Ceravolo** [ID] | **Francesco Tondolo** [ID]

Department of Structural, Geotechnical and Building Engineering (DISEG), Politecnico di Torino, Torino, Italy

Correspondence
Erica Lenticchia, Department of Structural, Geotechnical and Building Engineering (DISEG), Politecnico di Torino, Torino, Italy.
Email: erica.lenticchia@polito.it

Funding information
Getty Foundation

Abstract

Ferrocement is a type of thin wall-reinforced concrete composed of hydraulic cement mortar reinforced with several layers of steel wire mesh. The material is used as a low-cost construction and retrofit solution and allows the creation of very thin elements. In the past, the material was also used to build some structural engineering masterpieces that currently face preservation challenges. Despite the use of the material, few studies have analyzed its durability with respect to corrosion and its evaluation for preservation purposes. The paper presents the results of a testing campaign on ferrocement replica specimens subjected to a corrosive environment. After an aggressive aging procedure, where the specimens are exposed to chloride ingress, the specimens are tested through a four-point bending test to compare their performances. Results of the mechanical behavior are compared to the results from the half-cell potential monitoring carried out during the aging process and optical microscope acquisitions regarding the cross-sectional corrosion-loss area in the wires. The aim is to assess the performance of historical ferrocement exposed to degradation due to corrosion; this can be useful in identifying the best procedures to protect and preserve it, as well as in evaluating its performance over time.

KEYWORDS
cementitious composites, chlorides ingress, corrosion, durability, ferrocement

1 | INTRODUCTION

Degradation caused by corrosion of steel reinforcement is one of the main causes of the loss of performance of reinforced concrete and cementitious composites structures, adversely affecting their durability and service life and may eventually cause their failure.[1,2]

Contrary to building and structures built in the last decades that may have been protected with technical solution foreseen in the design stage, structures and architectures built in the first half of the twentieth century often do not present any protection, such as galvanization of steel, corrosion inhibitors additives, or protective coatings of the surfaces. Moreover, buildings and infrastructures built at the time, present other intrinsic fragilities with respect to their performance under environmental actions or degradation phenomena. In fact, in this time frame, the advent of new materials and construction techniques had an overwhelming impact on the experimentation by designers, who created solutions that

often turned out to be harmful or unsuitable to endure over time (e.g., reduced cover meter, use of new materials with unproven performance records, use of materials now identified as hazardous, total exposure of concrete surfaces, etc.). Moreover, the misplaced confidence that cementitious composites could last eternally caused many durability and conservation issues over time.[2–4]

Ferrocement is part of that series of materials and technological solution that was pioneered during this period. In the ACI Committee 549 state-of-the-art report of the material, first published in 1980 and still currently enforced, it's given the following definition of ferrocement: "Ferrocement is a type of thin wall reinforced concrete commonly constructed of hydraulic cement mortar reinforced with closely spaced layers of continuous and relatively small size wire mesh. The mesh may be made of metallic or other suitable materials",[5–7] and as Prof. Naaman undelight, the definition, while quite general, is surprisingly close to the initial definition of ferrocement described by the original Lambot, who patented the material in 1855.[8] However, its employment in civil construction was very limited; at the beginning, the material was used to build boat hulls, water container, and plant pots, until Pier Luigi Nervi recognized the possible advantages of the material.

Pier Luigi Nervi started to experiment with ferrocement in the 40s, following the necessity dictated by the autarchy period of reducing material quantities, in particular, by reducing the imposing steel savings in the building industry that were instead directed into armaments manufacture and military purposes.[9] From his experiments to minimize the use of steel and cut the amount of construction material, Nervi realized that ferrocement presented different advantages: he could mold concrete as some sort of steel material, thanks to the even distribution of the reinforcements throughout its thickness and in both directions and meshes did not face as strict a ban as larger reinforcing bars. Moreover, it required no formwork and a minimum of skilled labor. Starting first from prototype building,[10–12] Nervi in 1947 had the possibility to use his patented solution to create large span roofing systems in the commissioned pavilions of the Turin Exhibition Center in Torino, Italy. From that experience ferrocement started to be employed by Nervi, and then it widespread in the construction field. The construction methodology utilized prefabrication and avoided heavy machinery, resulting in faster and more economical construction compared to competitors.

Currently ferrocement is employed worldwide both as a construction material, or for retrofit reason (e.g., confinement jackets for reinforced concrete columns, reinforcement for unreinforced brick or masonry walls, etc.),[13–15] it advantages include a great formal freedom, making it possible to create different shapes and free form solutions, the low-cost of the materials employed (cement mortar and meshes).[8,16]

However, like other cementitious composites, it may present durability issues due to its construction feature which results, in particular, in a high surface area of reinforcement and limited thickness of the concrete cover.

In this paper, the performance of historical ferrocement specimens subjected to corrosive environments is evaluated by an experimental campaign carried out on ferrocement specimens. The ferrocement under analysis is the one employed by Nervi in the structures of Turin Exhibition Center (or Torino Esposizioni), built between 1947 and 1953.[11,12] In both pavilions ferrocement is used in different forms and solutions that Nervi patented in those years: such as the waved ashlars (Patent no. 445781 registered in August 1948) and the "tavelloni" (Patent no. 465636 registered on May 19, 1950).[17,18] Considering the historical value of the analyzed structures and since the ferrocement elements are extremely thin, which didn't allow for the use of any investigation tests, to investigate the durability of this material, small-scale ferrocement replica specimens were built in the laboratory, starting from a small sample collected on-site. More specifically, the sample was collected from one of the ferrocement beams elements of Hall C, which elements and investigation campaign are better described in Lenticchia et al.[19] The sample was used to determine the matrix composition of the concrete (both chemical and petrographically) and identify the wire mesh characteristics, in order to recreate the recipe employed originally by Pier Luigi Nervi.

The ferrocement samples built in the lab were then investigated by subjecting them to a corrosive environment. After an aggressive aging procedure, where the specimens are exposed to natural chloride ingress, the specimens are tested through a four-point bending test to compare their performances, by following the ACI recommendation.[6,7] Results of the mechanical performance are then compared to the results from the half-cell potential monitoring that was carried out during the aging process.

The insights given by the present work will be useful to identify the best procedures to protect and preserve this material, as well as evaluate its performance over time.

1.1 | Research significance

The material is largely used as a low-cost construction and retrofit solution and allows the creation of very thin elements. Despite the use of the material, few studies

have analyzed its durability with respect to corrosion[20–23] and research on the subject has been mostly restricted to ferrocement configurations, in terms of mixtures or wire mesh used, that were not present in the past (e.g., use of galvanized, or stainless-steel reinforcements).

In the past, the material was also used for the construction of some structural engineering masterpieces (e.g., the Sydney Opera House), some of which faced preservation challenges. Moreover, in literature, there is a lack of studies regarding the behavior of historical ferrocement elements, their state of preservation regarding loss of ductility, and their evaluation for preservation purposes.

Another issue that characterizes construction technology and consequently requires specific insights is the difficulty of inspecting it for diagnosis purposes. Due to the minimal thickness of the ferrocement elements, it is often not possible to carry out a proper diagnosis on-site. In fact, the most common non-destructive tests, such as georadar, ultrasonic pulse velocity, and rebound tests, failed to give any information or were not suitable since the analyzed ferrocement elements spanned from 2 to 4 cm thickness; the half-cell potential test also failed to provide any information since the continuity of the reinforcement somehow was not guaranteed. Moreover, given the position of the elements to be investigated and the fact that they were used as formwork for the concrete pouring, it was not possible to collect samples large enough to carry out any destructive test.

The present study wants to contribute to an unexplored area of research, whereas in the majority of cases, degraded structural elements built in ferrocement are demolished, the objective is to extend the service life of the material, in view of preserving a heritage belonging to the history of civil engineer. In engineering applications, this study is useful to identify the properties of historical/existing ferrocement elements and predict their capacity.

2 | MATERIALS AND METHODS

In order to investigate the performance of the historical ferrocement under analysis, the experimental campaign was structured into the following phases: (i) material investigation; (ii) samples reconstruction; (iii) samples aging; and (iv) samples monitoring and testing.

In the initial stage of material investigation, a sample was collected from the original structure under analysis to gather comprehensive data about its composition. The results of the mechanical, chemical, and petrographical analyses were used to recreate the specimens to be aged by exposing them to chloride ingress, in a wet and drying cycle. During the aging process, samples were monitored by means of photographic documentation and half-cell potential measurements.

At the end of the aging process, all samples are subjected to a four-point bending test until failure. The aim is to compare the results with samples that did not undergo aging to comprehend the impact of corrosion on the structural performance of the material.

2.1 | Investigation on materials

The ferrocement under analysis is the one employed by Nervi in the structures of Torino Esposizioni. In both pavilions ferrocement is used in different forms and solutions which Nervi patented in those years. Figure 1 shows the elements of the pavilions where ferrocement was employed. To replicate Nervi's ferrocement, and determine the proper mixture, it was fundamental to study the patents[24–27] and the writings authored by the designer,[10,12,18,28,29] as well as identifying all the ferrocement elements in the halls and their differences. From the original documentation alone, however, it was not possible to state with certainty the actual mix design of the recipe used by Nervi, especially to assert the one related to the structures under analysis.

Regarding direct investigation on the material, it was not possible to carry out a proper diagnosis on-site, apart from endoscopies and partial scarifications, due to the fact that ferrocement elements were presented a thickness below the minimum one requested by the most common non-destructive tests (such as ultrasonic pulse velocity, and rebound tests); another issue for on-site material investigation was due to the use of some ferrocement elements as formwork, where concrete was poured over them, and consequently it was not possible to investigate it.

When partial scarification was performed at the surface level, it exposed the first mesh layer of the ferrocement element. Usually, on visual analysis, the first layer of mesh was found to be partially affected by corrosion.

After these first analyses, the authors proceeded in collecting a sample of ferrocement by selecting the most feasible location: the beams elements of hall C. In fact, the corrugated slab at the impost of the vault consists of prefabricated ferrocement elements with a 9.5 m span with a wave section, then connected by in-situ casting to give continuity.

The corrugated beam consisted of a precise combination of reinforcement, with wire mesh and high-quality cement mortar. Its cross-sectional area was not constant but increased from the outside inward towards the arches, where it reached its maximum size (Figure 2a). The element was 0.94 m wide, 9.5 m long, as mentioned
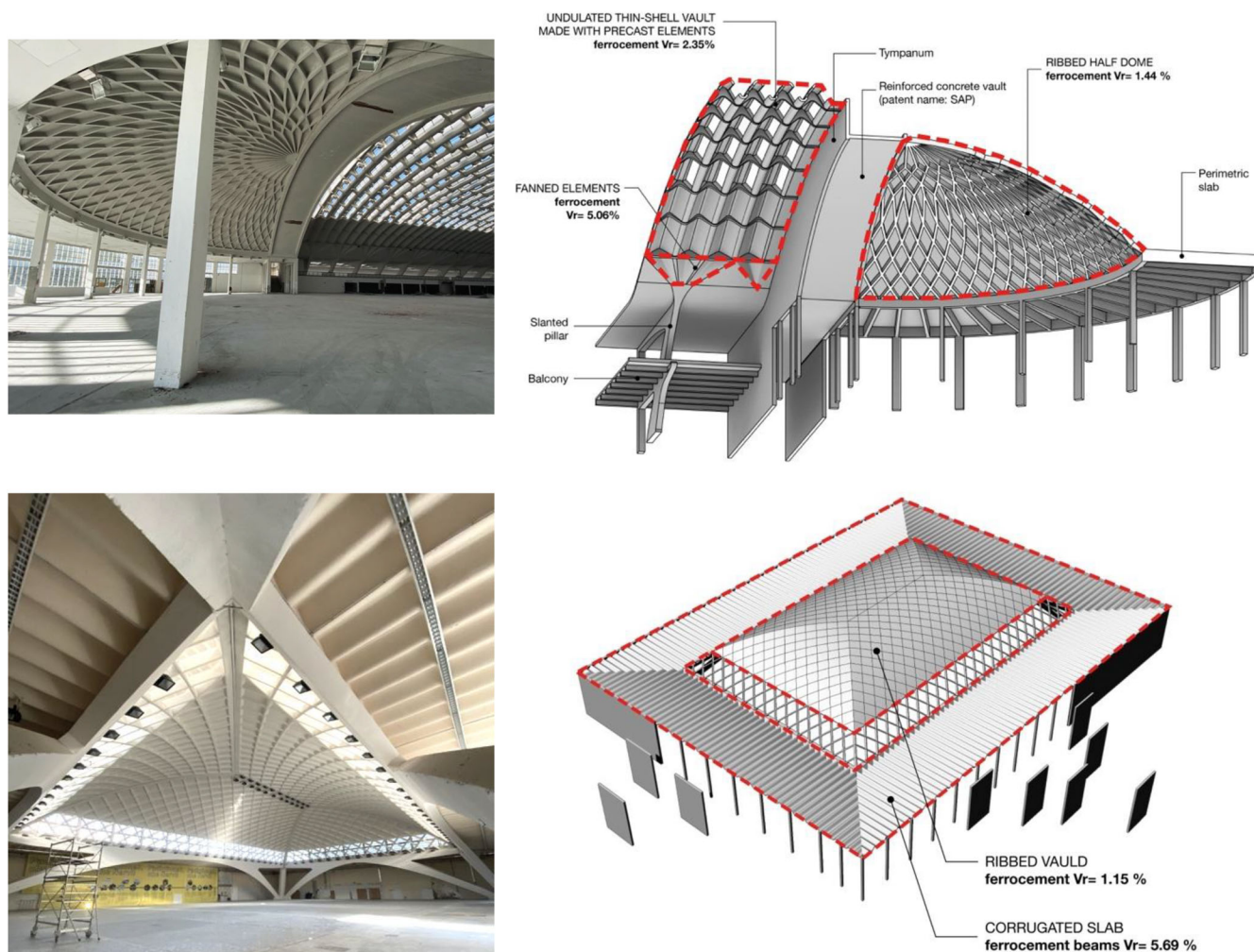
FIGURE 1 Interior view of Nervi's halls in Torino Esposizioni and their schematization showing where the main ferrocement elements are located and their volumetric steel fraction in percentage. On the top is reported the Hall B, while the Hall C is on the bottom.

before, and with a height ranging from 0.26 to 0.44 m at the highest part. It is a modular element with remarkable strength characteristics, despite its slight thickness (2–4 cm). From the original design, the internal reinforcement of the corrugated beam in Hall C consisted of three layers of wire mesh weighing 0.600 kg/m², both above and below the ordinary reinforcement, to form the characteristic curved shape[25,27,30] (Figure 2b).

The extracted sample was about 12 cm × 12 cm (Figure 3), from an undulated beam located in the west area of Hall C.[19] The sample was used to determine the cement composition and to analyze the actual number of mesh layers employed by Nervi and the wire characteristics. From the sample it was possible to assess that the ferrocement of the undulated beam of Hall C is constituted by four layers of mesh in 2 cm thickness, which bring to a steel—composite ratio of 3.14%. In fact, from the knowledge phase of both halls, it

emerged that Nervi employed different volumetric steel fraction depending on the structural element in ferrocement. Overall, the volumetric steel fraction, calculated thanks to the original drawings, is reported in Table 1, while Figure 1 reports their location. The volumetric steel fraction is estimated as the ratio between the steel area divided by the total transversal area of the concrete matrix. Regarding Hall C, it is important to highlight that the ferrocement of the undulated beams presented six layers (Figure 2a), while the extracted sample had only four of them. Moreover, Nervi in the volumetric steel fraction counted the contribution of the additional layer of reinforcement, constituted by small diameter bars, these differences are reported in Table 1.

Thanks to the extracted sample, it was possible to carry out the characterization of the materials in order to recreate the ferrocement of Nervi in the lab.
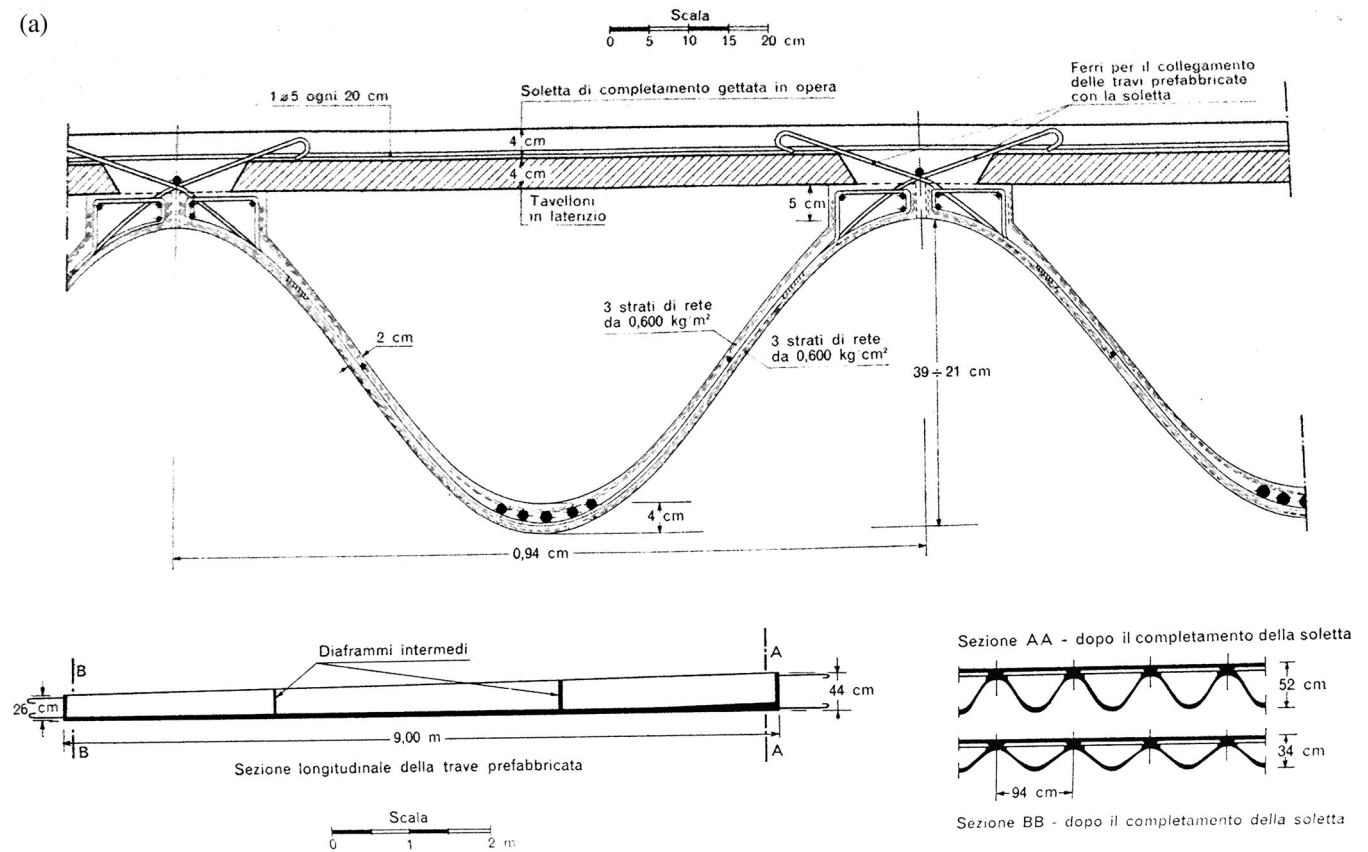
(a)

(b)

FIGURE 2   (a) Illustration of construction details related to ferrocement corrugated beams.[30] It is possible to appreciate the number of the wire mesh layers and the variations in thickness in the cross section. (b) Prefabrication on site of the undulated beams in ferrocement (1949–1950).[17]
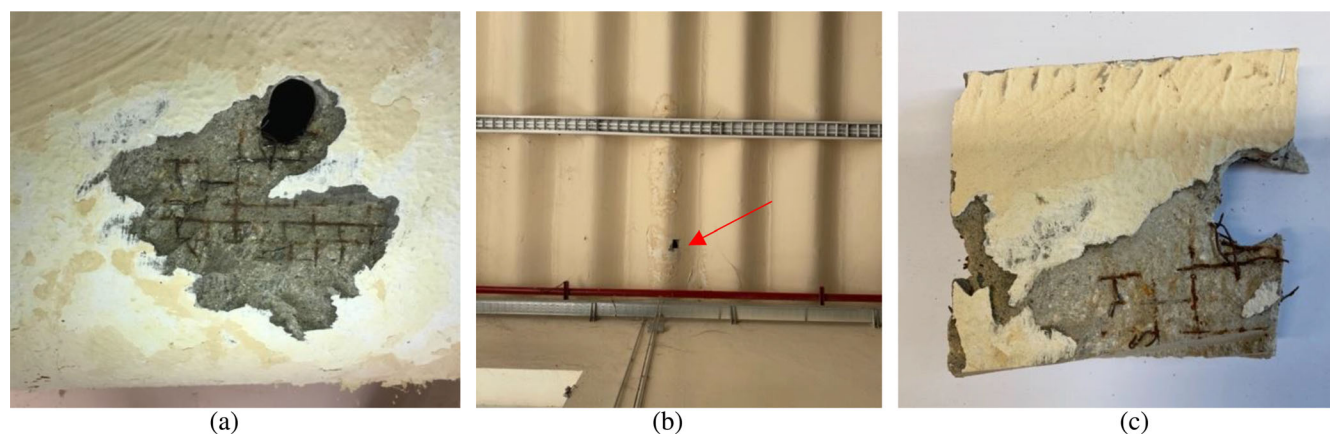
FIGURE 3 (a) Scarification of a ferrocement beam element located in Hall C, it is also possible to appreciate the trace for the endoscopy test; (b) location of the sample extraction, indicated with a red arrow; (c) extracted ferrocement sample.

TABLE 1 Volumetric steel fraction % in To-expo ferrocement structural elements based on the original drawings.

	Thickness (mm)	number of layers of steel mesh	Volume of the ordinary reinforcement (cm³)	Volumetric steel fraction (V_r) (%)
Elements—Hall B				
Undulated element	45	3	585.9	2.35
Fan-shaped element	35	3	1298.5	5.06
Diamond-shaped elements	10	1	130.9	1.44
Elements—Hall C				
Undulated beam (six layers of wire mesh)	20	6	196.4	5.69
Undulated beam (six layers of wire mesh without small diameter bars)	20	6	-	4.71
Undulated beam (four layers of wire mesh)	20	4	196.4	4.12
Undulated beam (four layers of wire mesh without small diameter bars)	20	4	-	3.14
Diamond-shaped elements	25	1	130.9	1.15

2.1.1 | Cement matrix

According to the results of the petrographic analysis and the chemical and mineralogical characterization, better reported in Ceravolo et al.,[31] the replica specimens were reconstructed by using a mortar based on pozzolanic cement prepared in the Buzzi Unicem mixing plant in Trino (VC). The pozzolanic component (in replacement of bentonite) confers to the mortar a thixotropic consistence, making it suitable to be set and modeled around the metallic mesh, with 60 min of workability time. Typical performances are compressive strength higher than 10, 35, and 45 MPa after 1, 7, and 28 days, respectively; flexural strength higher than 4, 6, and 8 MPa after 1, 7, and 28 days, respectively. As a measure of comparison regarding the compressive strength of the mortar with the original one, it was possible to collect some data regarding

the cement properties from the original laboratory certificates of the time containing data from the MASTRLAB Certificate Archive of the Politecnico di Torino—Turin Exhibition Center for the years 1947–1954. These data are published in the report regarding the conservation management plan of the halls.[32] It is important to highlight that any trace of possible additive organic nature couldn't be assessed, as well as the actual w/c ratio for the cement mortar employed by Nervi, so there are some intrinsic uncertainties. For what regards mortar, a w/c ratio of 0.18 was used, 160 mm × 40 mm × 40 mm samples are cast and tested by following the EN ISO 1015-11,[33] and performing a three-point bending test (Figure 4). Flexural testing separated the specimens into two halves, which were then tested in compression by applying a load without shock at a uniform rate at 50 N/s. The results of the mechanical tests on mortar are reported in Tables 2 and 3.
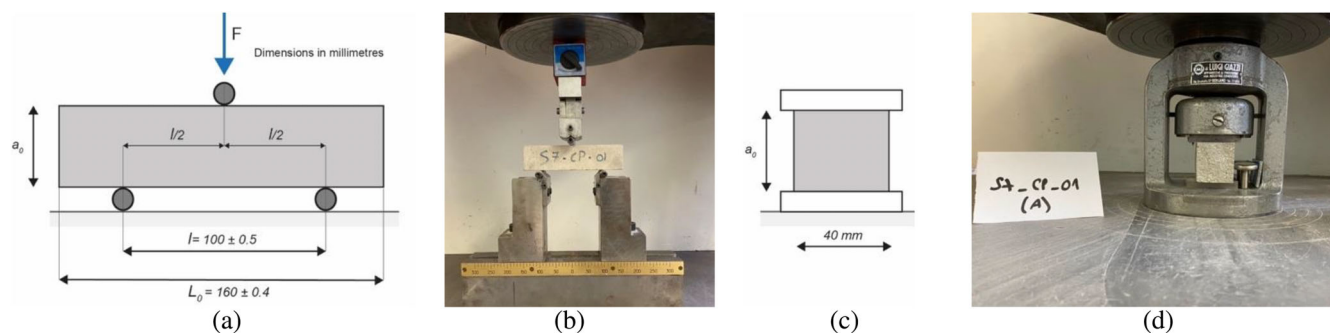
FIGURE 4   Setup of the characterization of the cement matrix: Scheme of the setup according to the EN ISO 1015-11 for the three-point bending test (a) and the actual test (b); scheme of the setup according to the EN ISO 1015-11 (c) and the compressive test (d).

TABLE 2   Results of the three-point bending tests on mortar specimens, reporting the IDs, the geometrical dimensions a_0 and b_0, the depth and width respectively, and the results in terms of load F_{max}, the obtained mean value, and standard deviation.

ID	a_0 (mm)	b_0 (mm)	F_{max} (N)
S7-CP-01	37.44	39.9	3029
S7-CP-02	39.40	39.89	3092
S7-CP-03	37.77	39.82	1530
S7-CP-04	39.78	39.98	3491
S7-CP-05	40.48	39.85	3080
S7-CP-06	39.62	39.87	3317
		F_{max} (mean) (N)	2924
		SD (N)	705

2.1.2 | Wire mesh steel

The extracted sample was also useful to determine the wire mesh used by Nervi. From a first visual analysis, the wires of the mesh in the location selected for sampling resulted corroded (Figure 3c). To better analyze the state of conservation and its characteristics, each layer of metal mesh was carefully removed from the cement matrix by using a hammer, chisel, and an electric abrasive. After removal, all layers extracted were documented and cataloged. The resulting steel meshes consist of interwoven steel wires (not welded) with a diameter of 1 mm and from handling it resulted to be mild steel. From this analysis and knowing the approximate characteristics of the steel chosen by Nervi at the time, thanks to the original technical reports, the reinforcements for the mock-ups were chosen, by selecting smooth steel bars and woven meshes with 1 mm diameter and 10 mm × 10 mm spacing. The chosen wires for the specimens were then tested by simple tensile test following the EN ISO 6892-1:2019[34] standards. Results are shown in Table 4, and reports the ID of the different tested wires, which dimension in terms of diameter

was measured in three different points (D1, D2, D3), in order to calculate the average diameter (Dm) of each wire.

2.2 | Samples construction

For evaluating the performance of the ferrocement, 11 samples are realized with a dimension of 300 mm × 75 mm × 30 mm, each sample included seven layers of metal mesh 270 mm × 55 mm (V_r = 3.63%). The dimension of the samples and the number of layers were defined by following Pier Luigi Nervi's design (regarding the volume fraction of steel reinforcement) and in accordance with ACI indications,[6,7] in order to use the proper dimensions for the mechanical tests.

The V_r value found in the sample extracted from the corrugated beam in Hall C is 3.14%. However, it should be considered that the thickness of the beam is variable, and the reinforcement is not distributed in the same way over the entire beam, and considering the entire section of the beam, including longitudinal and transverse reinforcing bars, the Authors find V_r = 4.12%. A representative value for the entire beam section can then be the average between the two, 3.63%.

The samples were poured by using a w/c ratio equal to 0.18, which provided the best workability for this application, and to obtain a good quality compact matrix to ensure good durability as highlighted by Naaman[8] stating that the w/c ratio shouldn't exceed 0.4–0.45 by weight. For lack of information, it was not possible to establish the w/c ratio employed by the designer. Figure 5 shows the construction phase of the samples, including the assembly of the steel connections for the half-cell corrosion potential measurements. All samples were then cured for 28 days underwater in a humidity-controlled environment. One of the samples was treated with a layer of water-based acrylic paint in order to better simulate the exposure situation in the halls (Figure 3).

TABLE 3 Results of compressive test on mortar specimens.

ID	S_0 (mm^2)	F_{max} (N)	σ_{max} (N/mm^2)
S7-CP-01-A	1600	84,810	53.0
S7-CP-01-B	1600	81,082	50.7
S7-CP-02-A	1600	88,260	55.2
S7-CP-02-B	1600	89,909	56.2
S7-CP-03-A	1600	83,198	52.0
S7-CP-03-B	1600	87,394	54.6
S7-CP-04-A	1600	95,663	59.8
S7-CP-04-B	1600	89,672	56.0
S7-CP-05-A	1600	83,767	52.4
S7-CP-05-B	1600	93,580	58.5
S7-CP-06-A	1600	91,465	57.2
S7-CP-06-B	1600	90,358	56.5
		σ_{max} (mean) (N/mm^2)	55.2
		SD (N/mm^2)	2.7

Note: S_0 is the area of compressed mortar during the test, computed considering standard dimension of the sample from EN ISO 1015-11.[33]

TABLE 4 Results of tensile strength test (σ) on steel wires selected for the ferrocement specimens.

| ID	D1 (mm)	D2 (mm)	D3 (mm)	Dm (mm)	F (N)	A (mm^2)	σ (N/mm^2)
w 01	1	0.998	1.031	1.01	260.60	0.80	325.7
w 02	0.988	1.032	1.041	1.02	260.91	0.82	319.3
w 03	0.993	0.989	1.003	1.00	260.94	0.78	335.8
w 04	1.002	1.018	0.985	1.00	260.78	0.79	331.1
w 05	1.001	0.988	0.992	0.99	260.43	0.78	336.0
w 06	1.001	0.999	0.99	1.00	259.58	0.78	332.9
w 07	0.997	1.014	0.99	1.00	261.76	0.79	333.2
w 08	1.005	1.007	0.987	1.00	261.34	0.78	333.1
w 09	1.006	1.022	1.015	1.01	259.36	0.81	321.1
w 10	1.016	1.007	1.025	1.02	259.28	0.81	320.0
						σ_m (N/mm^2)	328.8
						SD (N/mm^2)	6.66

Note: The mean value (σ_m) and the standard deviation of the results are also reported.
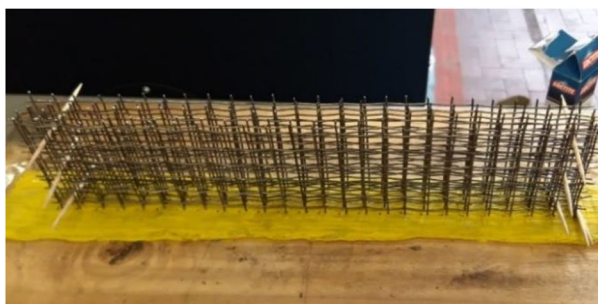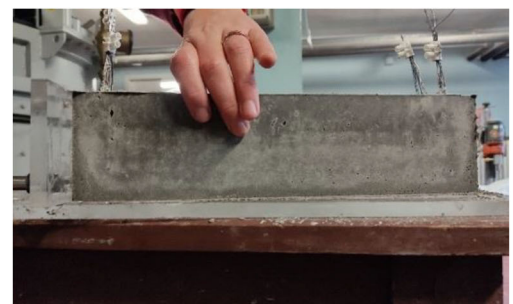
FIGURE 5 Ferrocement samples realization (a) net layers positioning (b) steel connections for subsequent corrosion potential measure (c) casted sample.

In order to rapidly appreciate the effect of corrosion, the samples were exposed to chloride ingress by placing the samples in a module where they were exposed to wet and dry cycles, and where during the wetting day, samples were sprayed continuously for 1 h employing a water solution with 3.5% NaCl. The drying occurred under natural conditions. No electrical current was applied. After 7 months of aging (precisely 201 days), all samples showed evident deterioration on the surface (Table 6).

2.2.1 | Expected ultimate load, simplified method using plastic moment

To evaluate the expected bending moment a simplified method using plastic moment is chosen. With this method, it is possible to assume the behavior of the section as a perfectly plastic elastic body with different properties in compression and tension. The properties in compression are those assumed in the ACI rectangular stress-block[6] (Figure 6); the properties in tension are defined by a value σ_{cy} which represents the yield of the composite material. In this case, all reinforcement layers are considered in the plastic field.

According to ACI Committee 549[6,8] to evaluate the bending moment with the simplified method, the following equations can be written:

$$C = 0.85 \cdot f'_c \cdot b \cdot a \tag{1}$$

$$T = \sigma_{cy} \cdot b \, (h-a) \tag{2}$$

where C, is defined as the compression force generated at the plastic limit, and T, as the tensile force generated at the plastic limit, while M_u, is the ultimate plastic bending moment.

Moreover, f'_c, represents the characteristic compressive strength of concrete, and, a, is the depth of rectangular

stress-block diagram, while, b, and, h, are the sample base and the sample's height, respectively. Table 5 and Figure 7 report the features of the samples analyzed in the present paper and the input data for calculating the expected resisting bending moment. The parameter σ_{cy}, is the tensile strength generated in ferrocement at the plastic limit.

$$\sigma_{cy} = \frac{\Sigma \eta \, V_{ri} A_c \sigma_{ryi}}{bh} = \Sigma \frac{A_{ri} \cdot \sigma_{ryi}}{b \cdot h} \tag{3}$$

$$a = \frac{\sigma_{cy} \cdot h}{0.85 \cdot f_c + \sigma_{cy}} \tag{4}$$

where η represents the efficiency factor of the mesh reinforcement, while, V_{ri}, is the volume fraction mesh in the volume i. A_c, is the cross-sectional area of ferrocement (composite section), while σ_{ryi} is yield strength of mesh reinforcement. A_{ri}, the effective cross-sectional area of reinforcement of layer i. So, the ultimate bending moment can be computed as:

$$M_u = (C \text{ or } T) \frac{h}{2} \tag{5}$$

Is possible to predict the simplified plastic moment from the Equation (5).

$$M_{ud} = 0.85 f'_c b a \frac{h}{2} = 124.89 \, \text{kN} \cdot \text{mm} \tag{6}$$

3 | EXPERIMENTAL PROCEDURE

Different tests were carried out during the aging procedure to monitor the development of the corrosion phenomena in the samples. In a photographic test campaign, regular and standardized photos were shot on a screen to develop superficial evidence of corrosion or other eventual phenomena on the samples.
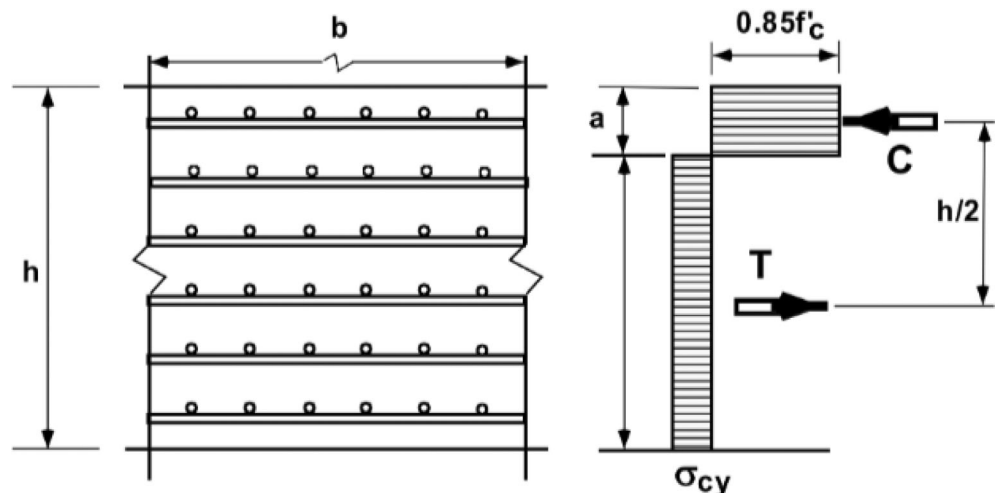

FIGURE 6 Plastic moment method.[8]

Half-cell potential test was measured on a regular grill of 20 points on each sample to keep track of the areas with a higher probability of corrosion development by using a standard anode immersed in copper sulfate.

In the end, sample performance was evaluated by carrying out four-point bending test, according to the ACI Committee 549[6,7] standards, and measuring the midspan deflection by means of an LVDT.

TABLE 5 Input data for expected resisting bending moment.

Input data		
n steel for each layer	5	$(-)$
n of layers	7	$(-)$
d_w	1	(mm)
b	75	(mm)
h	30	(mm)
i	3.67	(mm)
Concrete cover	4	(mm)
f'_c	55.17	(N/mm^2)
σ_s	328.8	(N/mm^2)
F points bending test arm	80	(mm)

The following paragraphs reports the results of each testing stage.

3.1 | Photographic campaign

Photographic test campaign is carried out each time with corrosion potential measurements, allowing the monitoring of the advancing of the corrosion process in the samples, giving a qualitative point of view of the aging process. Table 6 reports the photographic acquisitions of the samples at different time steps of the aging procedure.

3.2 | Corrosion potential

Half-cell corrosion potential measurements are carried out with a Cu/CuSO$_4$ reference electrode (Figure 8a). Half-cell corrosion potential is measured before starting the aging cycle, and every 2 weeks, during the aging process. All the data collected are evaluated in accordance ASTM C876 Guidelines[35] for corrosion potential of reinforcement steel without cover in concrete. The values are evaluated as follows:
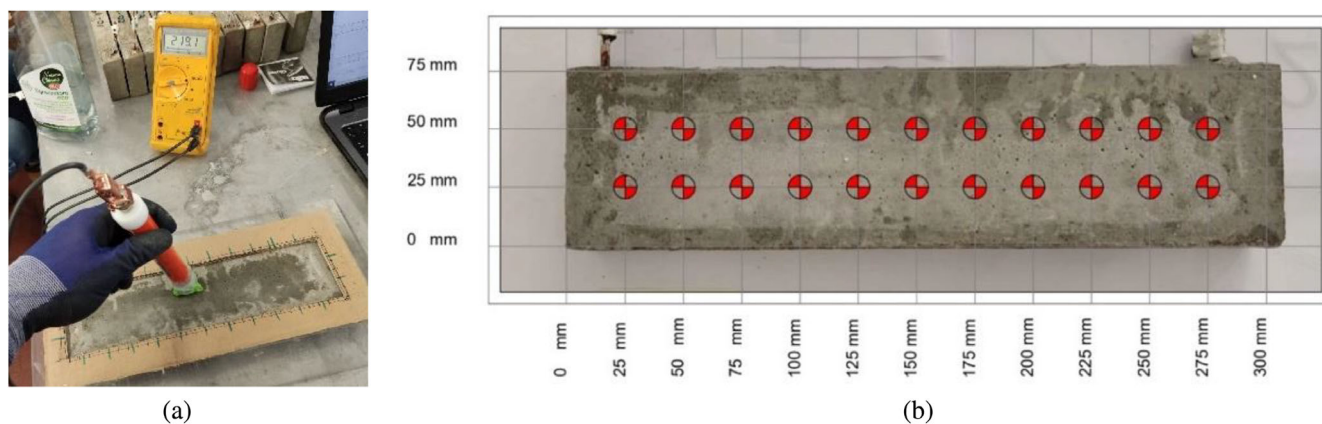

(a)   (b)

FIGURE 7 Ferrocement samples geometrical characteristics seen from: Front view (a) and longitudinal section (b). It is possible to appreciate the numbers of layers and the dimension of the samples.

TABLE 6 Pictures of the samples before and after aging.

Time	Aged_01	Aged_02	Aged_03	Aged_04	Painted and aged
t0 19/05/22 0 [d]					
t1 06/09/22 110 [d]					
t2 02/11/22 167 [d]					
tf 06/12/22 201 [d]					

FIGURE 8 (a) Corrosion potential measurement. (b) Corrosion potential measurements scheme showing the 20 points of acquisition.
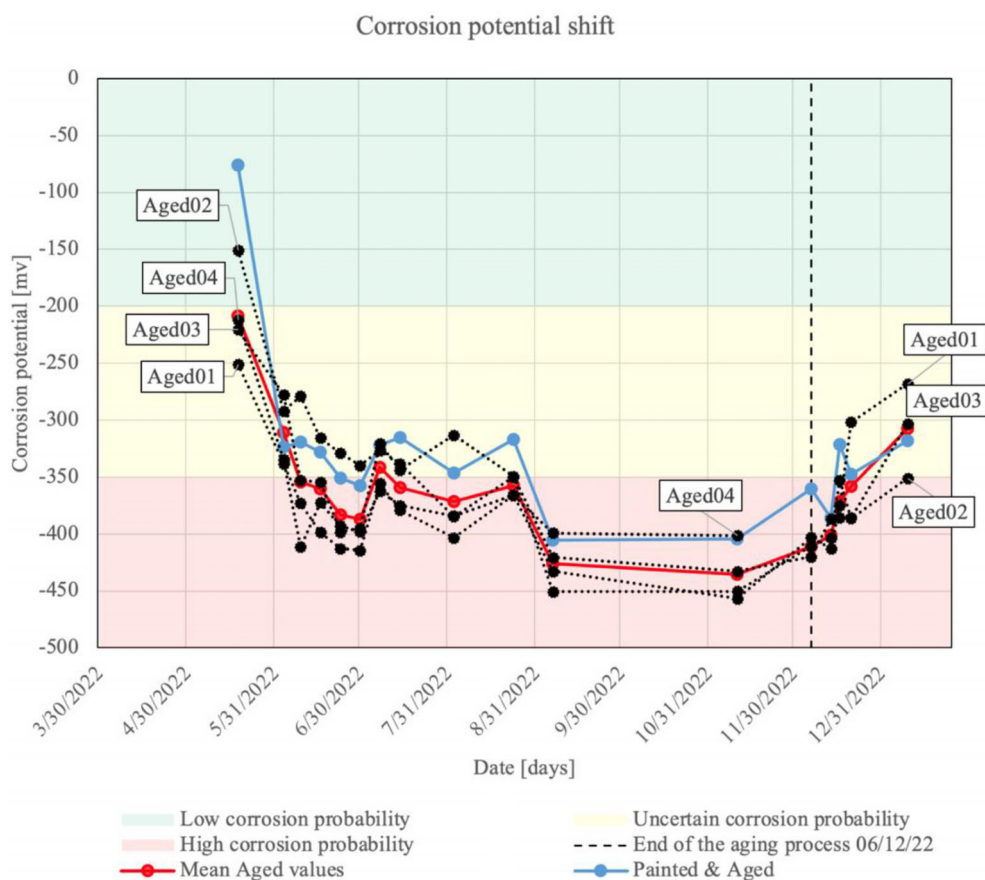

FIGURE 9 Corrosion potential shift the samples monitored during the 6 months aging period. The dotted line represents the stopping point of the aging process, after which the specimens were left to dry in a protected environment. One of the samples was treated with a layer of water-based acrylic paint in order to better simulate the exposure situation in the halls.
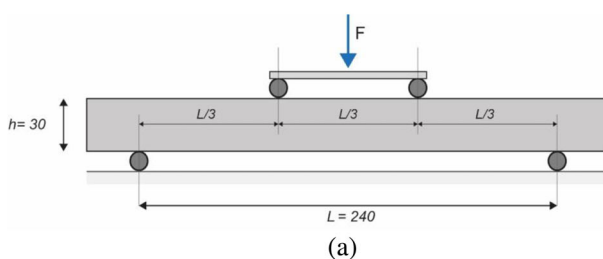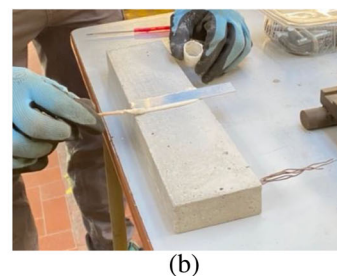

FIGURE 10 Setup of the four-point bending test, according to the configuration as required by ACI standards[6] (a); sample preparation (b).

- if corrosion potential is higher than -200 mV (with reference to Cu/CuSO$_4$), the probability of corrosion activity of the steel reinforcement is less than 10%.
- if corrosion potential is between -200 and -350 mV (with reference to Cu/CuSO$_4$), there is uncertain probability of the probability of corrosion activity of the steel reinforcement in the tested area.
- if corrosion potential is lower than -350 mV (with reference to Cu/CuSO$_4$), the probability of corrosion activity of the steel reinforcement is higher than 90%.

Twenty-two measurements are collected based on a 25 mm equally spaced grid on the surface of the sample

(Figure 8b). Before performing the measurements, the treated surface is wetted by spraying water.

The results of the half-cell potential tests carried out during the aging procedure are depicted in Figure 9. The dotted line represents the stopping point of the aging process, after which the specimens were left to dry in a protected environment. It is important to highlight that half-cell corrosion potential measurements were used to monitor changes in the performance of the samples during time. It has been largely demonstrated that half-cell potential tests carry out large uncertainties and are greatly affected by environmental conditions and other factors.[1] To overcome as much as possible this bias, the singles measurements values were taken as a mere
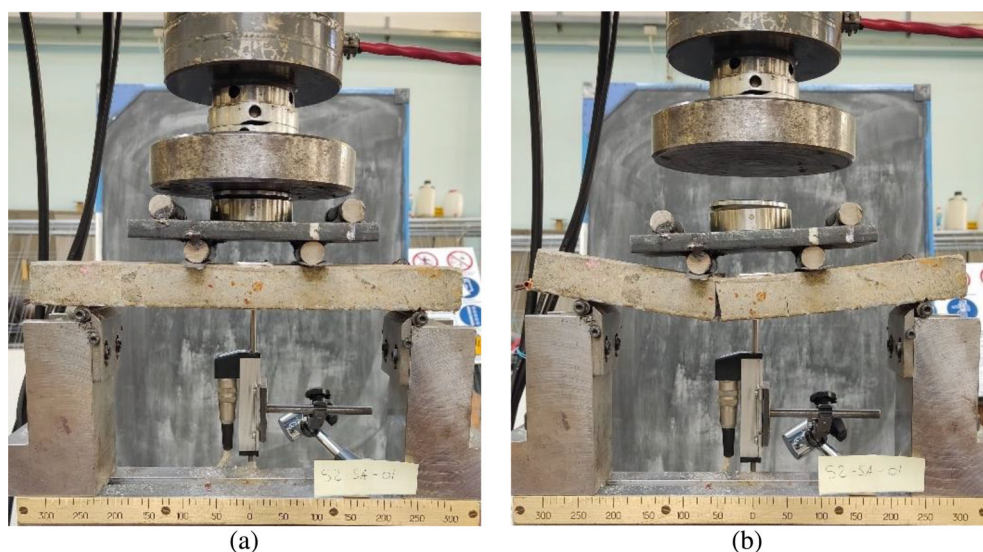
FIGURE 11 Four-point bending test (a) sample Aged_2 before the test (b) sample Aged_2 after the test.
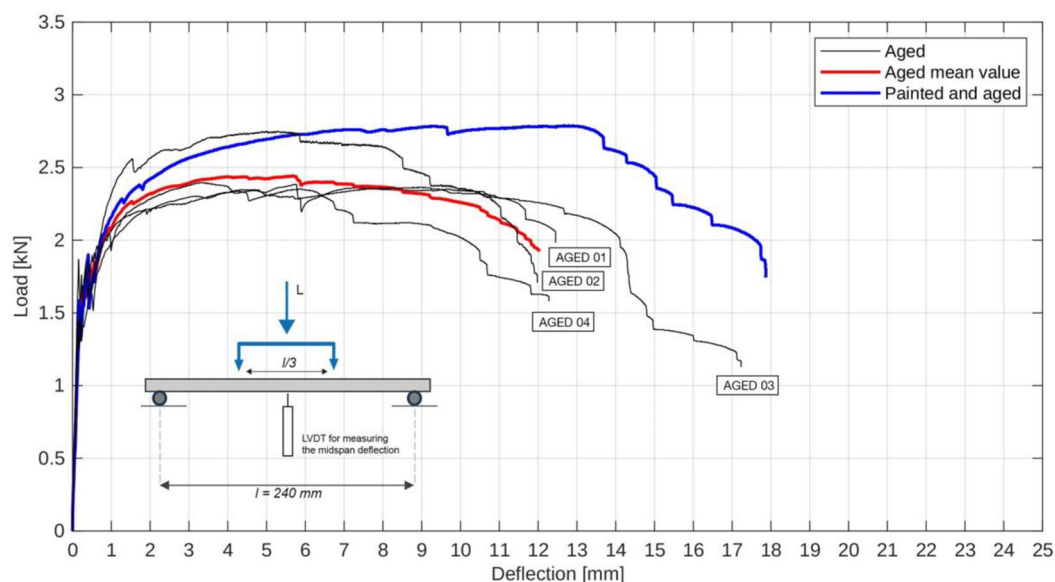
FIGURE 12 Four-point bending test load-deflection pattern, aged + painted and aged samples.

qualitative indication, while more importance was given to the trends of the measurements.

3.3 | Flexural test on ferrocement

Deterioration or loss of strength due to reinforcement corrosion can indicate relative corrosion damage. In order to evaluate it, all specimens were tested up to failure in flexure to evaluate changes in their performance, and consequently the effect of corrosion in the structural response. Flexural tests were carried out with the configuration as required by ACI Committee[6,8] with simply supported beam with third-point loading. For aged samples, the tested element was positioned with the side exposed to the aging process downward, subjected to tension state. Figures 10 and 11 show the setup of the four-point bending test. For the midspan displacement measurements by means of LVDT, a plate was assembled in the middle of each sample (Figure 10b). Figures 12 and 14 depict the load-deflection pattern for the aged and the non-aged series, respectively. In both figures, the mean value of the series is depicted with a red line, while the blue line always depicts the sample treated with a layer of paint.
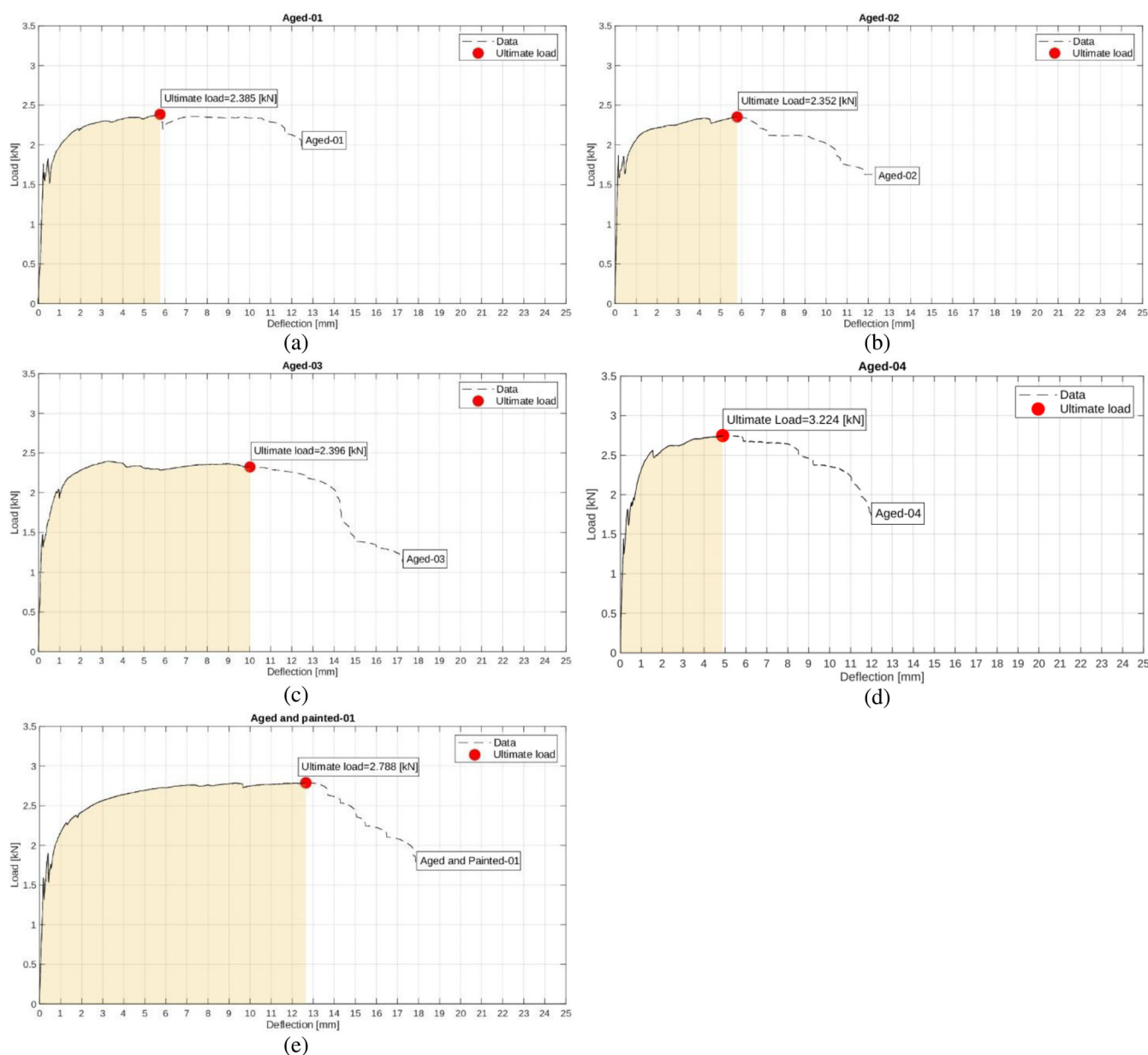
FIGURE 13 Four-point bending test load-deflection pattern with ultimate load point and work highlighted, aged samples from (a) to (d), painted and aged (e).
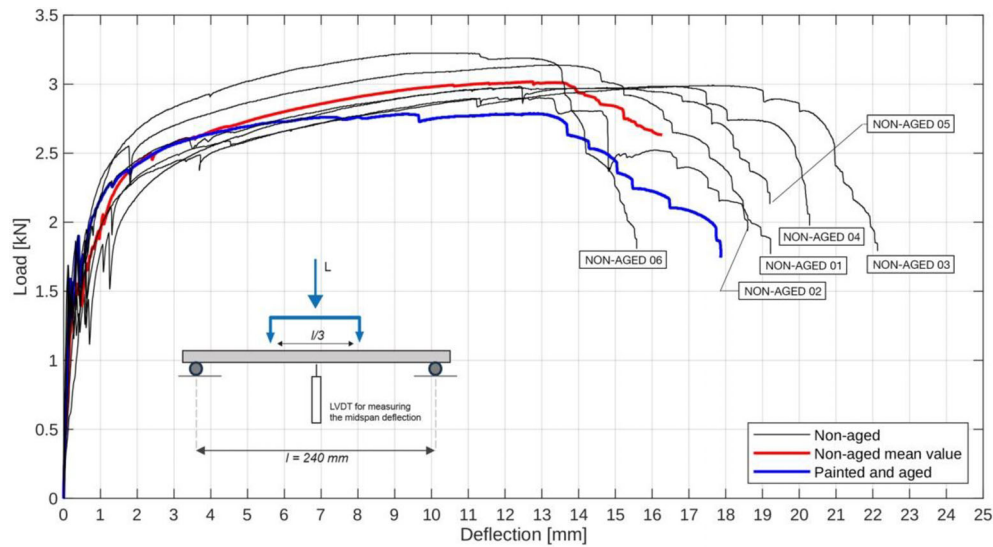
FIGURE 14 Four-point bending test load-deflection pattern, non-aged samples + painted and aged.
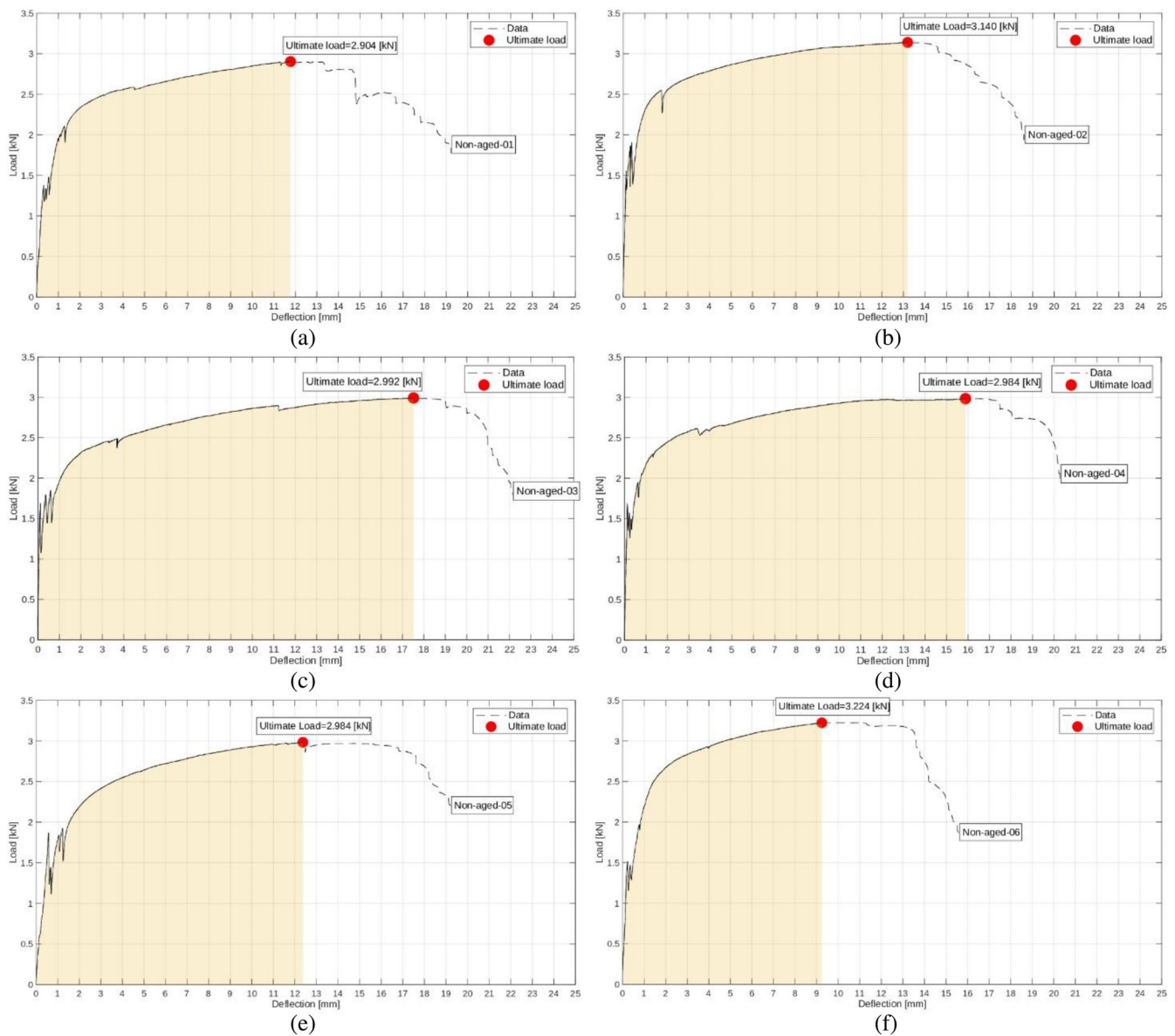

FIGURE 15 Four-point bending test, load-deflection pattern with ultimate load point and work highlighted, non-aged samples from (a) to (f).
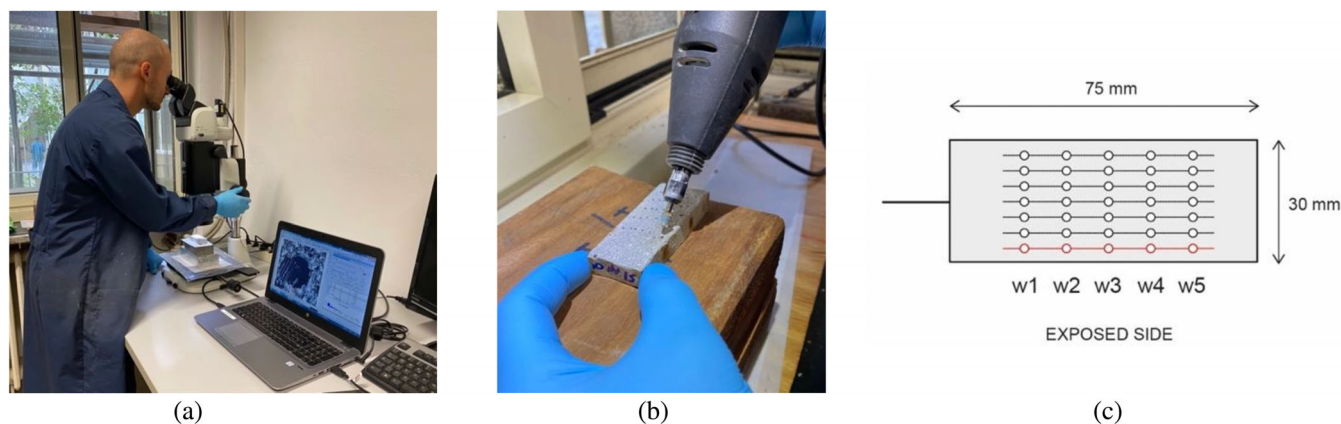
(a) (b) (c)

FIGURE 16 The employed microscope for the corrosion-loss estimation (a); mechanical cleaning of the extracted slice (b); scheme showing the cross section of the sample and the wire numbering (c).
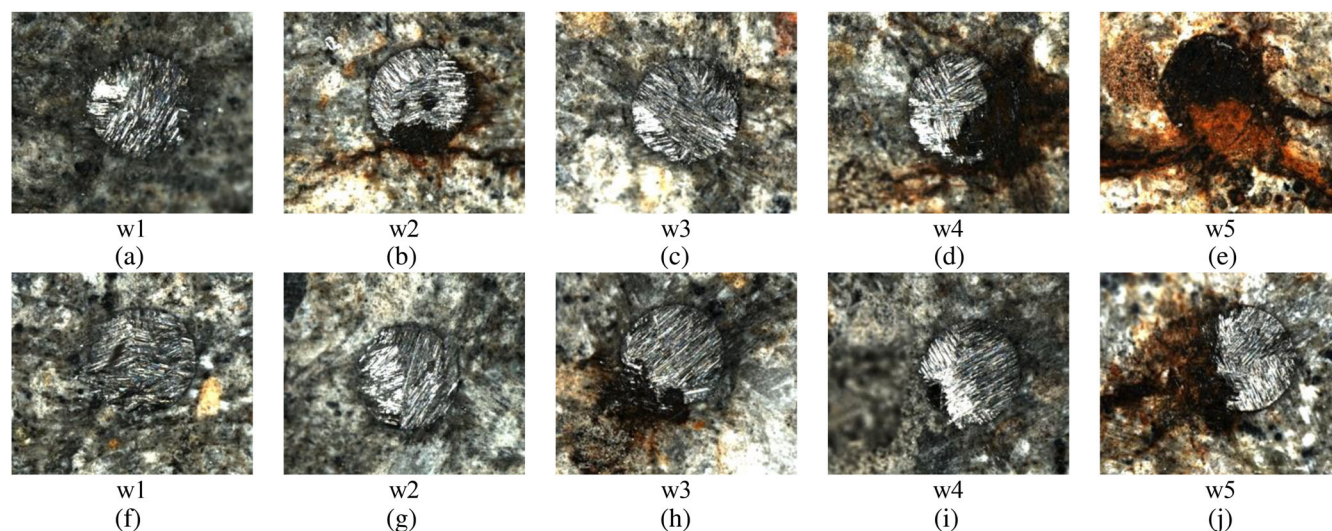

w1	w2	w3	w4	w5
(a)	(b)	(c)	(d)	(e)
w1	w2	w3	w4	w5
(f)	(g)	(h)	(i)	(j)

FIGURE 17 Photographic acquisitions of the corrosion state of wires of sample Aged_02 (a–e) and the painted and aged sample (f–j), by means of the optical microscope (magnification 5×).

FIGURE 18 Magnification of wire w5 of the sample presenting a layer of paint (painted and aged), magnification 2× (a) and 5× reporting the radius of the wire and the measured loss of area due to corrosion (b), respectively.

(a) (b)
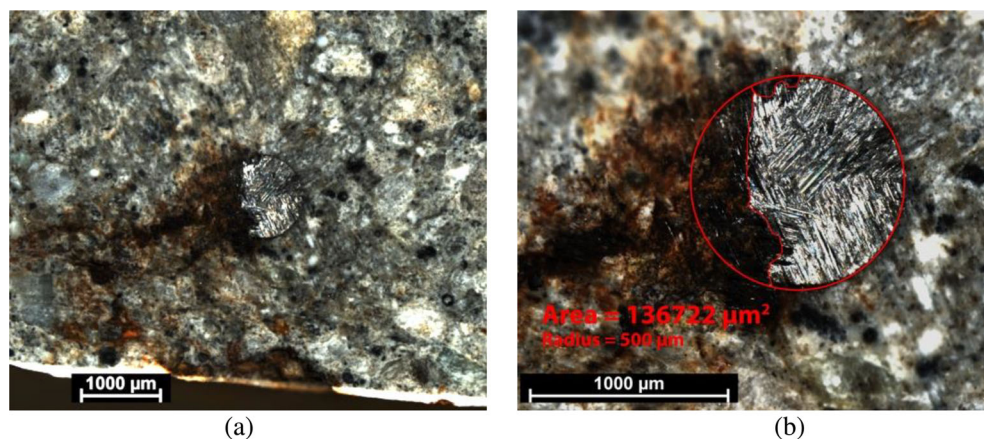
Table 9 reports the results of the flexural tests of aggregated samples in terms of ultimate load and ∂_u (defined as the deflection at the ultimate load). Results are used to evaluate the mechanical properties of the ferrocement samples by comparing the performance of the aged and non-aged ones. Table 10 reports the results in terms of mean values and their standard deviation for each parameter (ultimate load, work, and ∂_u). The comparison is done in terms of percentage loss compared to the non-aged samples; moreover, an additional parameter useful to evaluate the ductility of the material is by comparing the loss of work, which is represented by the underlying area of the load-deflection (Figures 13 and 15).

This loss in ductility can also be appreciated by the distribution of the crack pattern, and the crack width in the tensile zone (Table 7). In fact, the non-aged samples present a more distributed spread with respect to the non-aged ones.

3.4 | Corrosion-loss measurements

To better evaluate the effect of the corrosion, the cross-sectional corrosion-loss of the wires was estimated by using a stereoscope (Figure 16a). Following the mechanical test, a slice close to the main crack was extracted for each aged sample (Figure 16b). The slices were cleaned for the optical microscope observations, and it was observed that the corrosion occurred in the wires of the first layer of the exposed surface to chlorides of each sample (Figure 16c).

The corrosion was then measured for each wire of the first layer of mesh (highlighted in red in Figure 16c), which was the one closest to the surface exposed to the aging action of the chlorides. Figure 17 shows the photographic acquisition of the corrosion state of the wires of sample Aged_02 and the sample Aged and painted. Corrosion was detected in all samples, besides the different levels of seriousness in the different wires, ranging from no corrosion (e.g., Figure 17a,c, f,g,h) to the total corrosion of the area (Figure 17e). Results of the measurements of the cross-sectional corrosion-loss of the wires of each sample are reported in Table 8, while Figure 18 shows a detail of the measuring on a wire.

4 | DISCUSSION OF THE RESULTS

Comparing the mean ultimate bending moment at failure M_u obtained experimentally for the non-aged samples and the expected ultimate load from plastic moment M_{ud} (Equation 6), the difference is about 2.7%.

As it was highlighted from the previous paragraph, and from Tables 9 and 10, it is possible to notice an important difference from the aged and the non-aged series, especially by comparing the average maximum work and the corresponding displacement applicable to the samples.

In particular, with reference to the previous table, it is possible to compute the average loss in ultimate bending
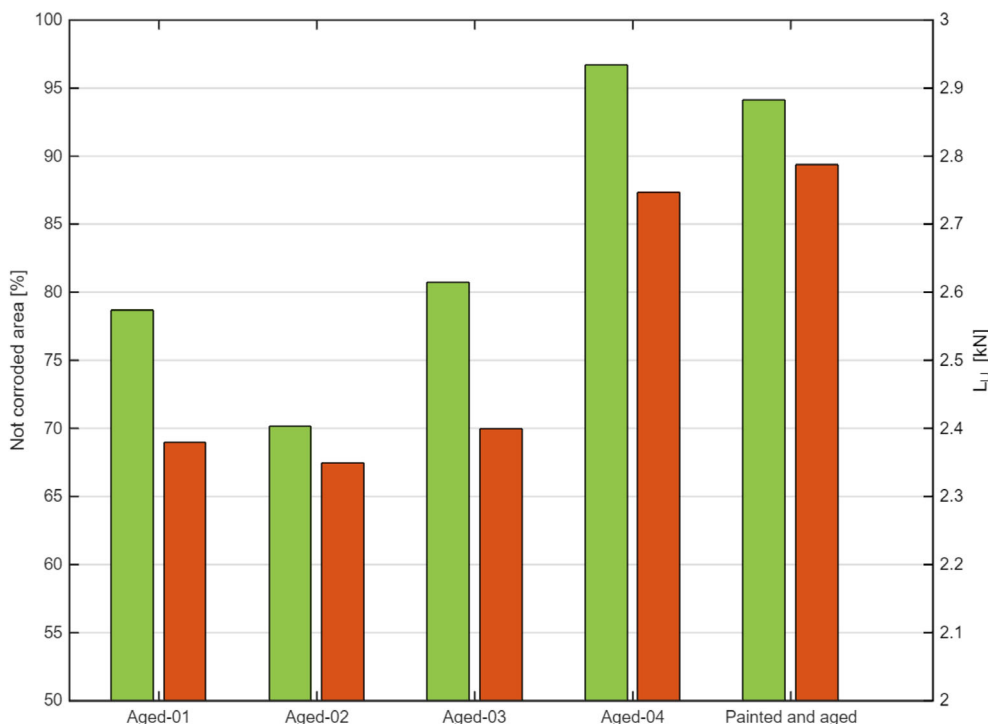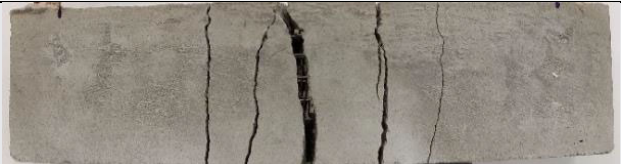

FIGURE 19 Comparison of the corrosion of the wires (in green), by considering the remaining area of the most exposed layer of mesh, with the load-bearing capacity obtained for each sample (in orange).

TABLE 7 Samples crack pattern after four points bending tests, from (a) to (d) aged samples, (e) painted and aged, from (f) to (j) non-aged samples.

moment $M_{u,loss}$, ultimate deflection $\delta_{u,loss}$, and the work loss $W_{u,loss}$ as:

$$M_{u,loss} = \frac{M_{u,nonaged} - M_{u,aged}}{M_{u,nonaged}} \quad (7)$$

$$\delta_{u,loss} = \frac{\delta_{u,nonaged} - \delta_{u,aged}}{\delta_{u,nonaged}} \quad (8)$$

$$W_{u,loss} = \frac{W_{u,nonaged} - W_{u,aged}}{W_{u,nonaged}} \quad (9)$$

Results are reported in Table 11, and it is possible to notice how aged samples show an important reduction of M_u, of about 18.7%, a significant statistical reduction of δ_u, of about 63.6%, and an average loss of W, of about

TABLE 8 Results of the measurements carried out using the stereoscope to measure the cross-sectional corrosion-loss area in the wires.

ID	Wire n	Area loss (μm^2)	Area loss (%)	Area loss tot[a] (mm^2)	Area loss tot[a] (%)	Remaining area (μm^2)	Total remaining area[a] (mm^2)
Aged 1	w1	513,625	65.40	0.834	21.25	271,773	3.092
	w2	43,376	5.52			742,022	
	w3	209,187	26.63			576,211	
	w4	0	0.00			785,398	
	w5	68,221	8.69			717,177	
Aged 2	w1	0	0.00	1.171	29.82	785,398	2.756
	w2	125,952	16.04			659,446	
	w3	0	0.00			785,398	
	w4	259,568	33.05			525,830	
	w5	785,398	100.00			0	
Aged 3	w1	194,042	24.71	0.756	19.24	591,356	3.171
	w2	68,664	8.74			716,734	
	w3	142,347	18.12			643,051	
	w4	167,916	21.38			617,482	
	w5	182,573	23.25			602,825	
Aged 4	w1	0	0.00	0.128	3.26	785,398	3.799
	w2	0	0.00			785,398	
	w3	0	0.00			785,398	
	w4	83,931	10.69			701,467	
	w5	44,271	5.64			741,127	
Painted and aged	w1	0	0.00	0.230	5.85	785,398	3.697
	w2	0	0.00			785,398	
	w3	93,128	11.86			692,270	
	w4	0	0.00			785,398	
	w5	136,722	17.41			648,676	

[a]The results refer to the wires in the same row, as highlighted in Figure 16a.

TABLE 9 Four-point bending test results.

ID	Ultimate load L_u (kN)	Ultimate moment M_u (kN · mm)	δ_u (mm)	Work (J)
Aged 1	2.38	95.4	5.762	12.379
Aged 2	2.35	94.0	5.778	12.564
Aged 3	2.40	95.8	3.268	6.763
Aged 4	2.748	109.9	4.88	11.934
Non-Aged 1	2.904	116.16	11.8	29.778
Non-Aged 2	3.14	125.6	13.4	37.317
Non-Aged 3	2.992	119.68	17.53	46.881
Non-Aged 4	2.984	119.36	16.7	43.308
Non-Aged 5	2.984	119.36	12.41	31.551
Non-Aged 6	3.224	128.96	9.248	25.942
Painted and aged	2.788	111.52	12.69	32.830

TABLE 10 Four-point bending test results, in terms of mean values of the different series.

Series	Mean L_u (kN)	SD L_u (kN)	Mean δ_u (mm)	SD δ_u (mm)	Mean W (J)	SD W (J)	Mean M_u (kN · mm)	SD M_u (kN· mm)
Aged	2.470	0.161	4.922	1.022	10.910	2.405	98.810	6.447
Non-aged	3.038	0.109	13.515	2.847	35.797	7.450	121.520	4.348
Painted and aged	2.788	-	12.690	-	32.831	-	111.520	-

TABLE 11 Four-point bending test, percentage of loss of mechanical properties, mean values for series.

| ID series	% M_u loss	% ∂_u loss	% W loss
Aged	18.688	63.580	69.521
Painted and aged	8.229	6.102	8.285

69.5% for the aged series. Moreover, the painted sample shows a lower decrease of values of M_u loss, 8.2%, and a notably lower reduction of δ_u (6.1%) and W (8.3%) values compared to aged samples that did not present a layer of paint.

From the results obtained by the experimentations, it can be stated that the sample presenting a layer of paint presents a behavior comparable to the one of not aged samples, with a slight decrease of performances, mostly evidenced by the W loss. This demonstrates very good

properties of protection that just a layer of paint can exert on this material. This is important for our observations and analysis, since most of the ferrocement elements located in the case under analysis present at least one of the surfaces protected with a thin layer of paint (Figure 3).

This is also confirmed by the results of the half-cell potential monitoring tests, where the higher rates of corrosion potential shift are found in the non-treated samples. Although, after the end of the aging process, a corrosion potential shift from values with high corrosion probability (below -350 mv) to values with uncertain corrosion probability (over -350 and below -250 mv) is noticed in all the samples, the painted one presents higher values during the whole aging process.

By considering the results of the optical microscope acquisitions it is also possible to compare the sectional corrosion of the wires with the load-bearing capacity

TABLE 12 Samples section after aging and four-point bending test, from (a) to (d) aged, (e) Painted and aged (the red arrows indicate the sample's side exposed to aging, subjected to tension during the four-point bending test).

Aged 01	Aged 02	Aged 03	Aged 04	Painted and Aged
(a)	(b)	(c)	(d)	(e)
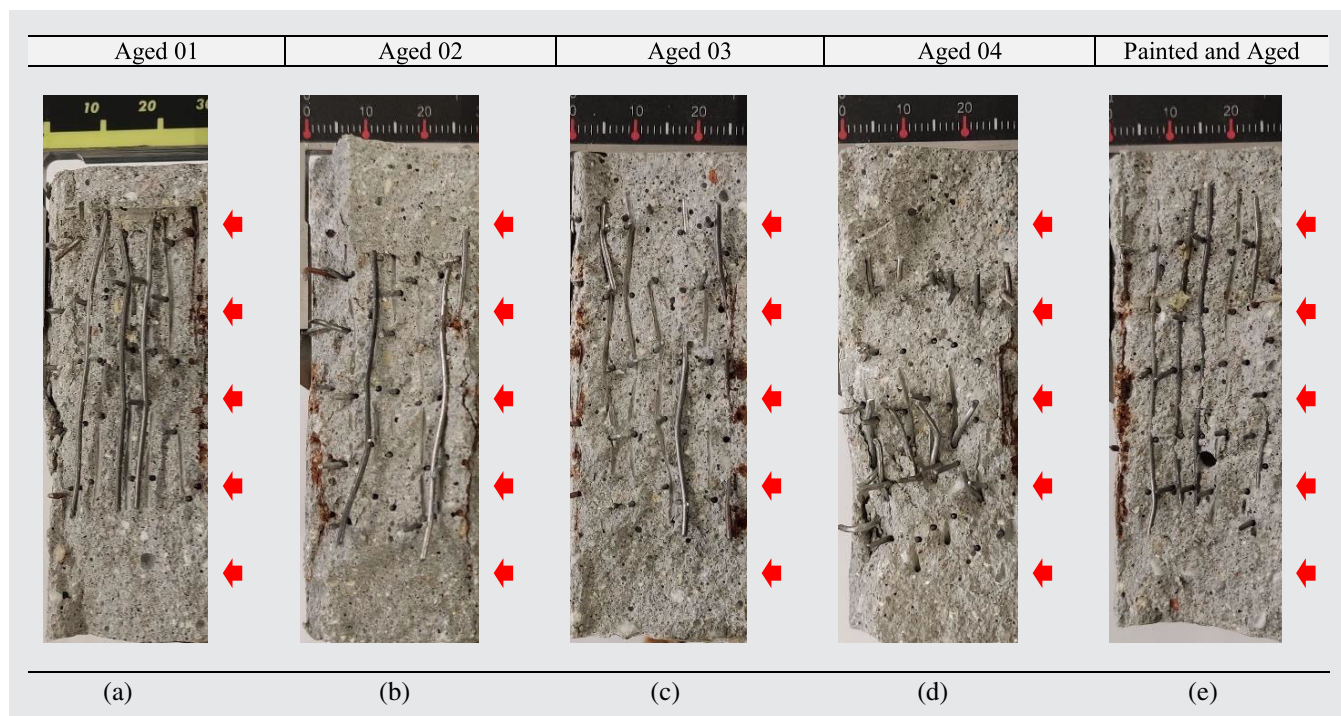
obtained for each sample. The comparison is showed in Figure 19, and it is possible to observe that in terms of ultimate load there is a correspondence between the amount of remaining area and the increase in the load capacity. It is important to note that the measurement of corrosion loss should be made at the point of rupture of the samples. However, it would be altered by the effect of the rupture itself. So, it is only possible to measure what happens in the vicinity of the rupture zone.

Moreover, the rupture sections of the aged samples, reported in Table 12, confirm how corrosion generally affected the first layer of reinforcement and, in some points (Table 12b), even the second layer. At failure, the ferrocement wires of the first layer were broken in different points, but by observing the load-deflection graphs (Figure 13) it is possible to assert that slip have occurred, especially considering the characteristics of the employed mesh (smooth wires of steel and not welded texture) also enhanced by the presence of corrosion.

5 | CONCLUSIONS

The study presented the behavior of ferrocement subjected to a corrosive environment; in particular, by reconstructing and analyzing the historical ferrocement used by Pier Luigi Nervi in his structures and carrying out both monitoring by means of half-cell potential and bending tests the performance of the material was evaluated. The aim was to understand the effects of aging on this material. The study is of interest since, despite the widespread use of the material, few studies have analyzed its durability for preservation purposes. Through a combination of a specific experimental campaign, which included photographic documentation, half-cell potential monitoring, mechanical tests, and stereoscope acquisitions to evaluate the corrosion-loss, we observed the development of the aging process, and we could evaluate how it affected the performance of the material.

Results of the experimental campaign suggest that a layer of painting, was efficient in protecting the material to the corrosive environment. However, the present work has only considered the degradation by subjecting the specimens to accelerated corrosion due to chloride ingress. Future works should be carried out to evaluate different degradations considering also carbonation. Moreover, other protections measures, such as corrosion inhibitor, or protective treatments of various nature, could also be investigated.

As also highlighted by,[36] since the research on the durability of ferrocement is still limited, it is difficult to predict the residual service life of the material after surface treatment. Moreover, research about the proper application and concentration of these treatments with regard to the porosity and penetration depth must be carried out.

AUTHOR CONTRIBUTIONS

ACKNOWLEDGMENTS

DATA AVAILABILITY STATEMENT

The data that support the findings of this study are available from the corresponding author upon reasonable request.

ORCID

Erica Lenticchia https://orcid.org/0000-0002-3746-2933
Rosario Ceravolo https://orcid.org/0000-0001-5880-8457
Francesco Tondolo https://orcid.org/0000-0003-0258-3054

REFERENCES

1. Bertolini L, Elsener B, Pedeferri P, Polder R. Corrosion of steel in concrete: prevention, diagnosis, repair. Germany: Wiley-VCH; 2005. https://doi.org/10.1002/3527603379
2. FIB. Fib model code for concrete structures 2010. Weinheim, Germany: Wiley-VCH Verlag GmbH & Co. KGaA; 2013. https://doi.org/10.1002/9783433604090
3. Harboe G, de los Monteros FE, Landi S, Normandin KC. The Cádiz document: innovaconcrete guidelines for conservation of concrete heritage. 2021.
4. Macdonald S, Gonçalves APA. Conservation principles for concrete of cultural significance. Los Angeles: Getty Conservation Institute; 2020.
5. ACI Committee 549. Guide for the design, construction, and repair of ferrocement. ACI Struct J. 1988;85(3):3527. https://doi.org/10.14359/3527
6. ACI Committee 549. Design guide for ferrocement. 2018:1–28.

7. ACI Committee 549. Report on ferrocement. 2018:1–20.

8. Naaman AE. Ferrocement and laminated cementitious composites. Ann Arbor, MI: Techno Press; 2000.

9. Leslie T. Beauty's rigor: patterns of production in the work of Pier Luigi Nervi. Champaign, IL: University of Illinois Press; 2017. https://doi.org/10.5406/j.ctt1vw0s2n

10. Greco C. The 'ferro-cemento' of Pier Luigi Nervi the new material and the first experimental building. Proceedings of the IASS, Padova. 1995.

11. Nervi PL. Concrete and structural form. Struct Eng. 1956;5: 155–72.

12. Nervi PL. Il Ferro-Cemento: Sue Caratteristiche e Possibilità. L'Ingegnere. 1951;1:17–25.

13. Aules WA, Saeed YM, Al-Azzawi H, Rad FN. Experimental investigation on short concrete columns laterally strengthened with ferrocement and CFRP. Case Stud Constr Mater. 2022;16: e01130. https://doi.org/10.1016/j.cscm.2022.e01130

14. Kadam SB, Singh Y, Li B. Out-of-plane behaviour of unreinforced masonry strengthened using ferrocement overlay. Mater Struct. 2015;48(10):3187–203. https://doi.org/10.1617/s11527-014-0390-8

15. Kaish ABMA, Jamil M, Raman SN, Zain MFM, Nahar L. Ferrocement composites for strengthening of concrete columns: a review. Constr Build Mater. 2018;160:326–40. https://doi.org/10.1016/j.conbuildmat.2017.11.054

16. Naaman AE. Evolution in ferrocement and thin reinforced cementitious composites. Arab J Sci Eng. 2012;37(2):421–41. https://doi.org/10.1007/s13369-012-0187-4

17. Gargiani R, Bologna A. The rhetoric of Pier Luigi Nervi: concrete and ferrocement forms. Treatise on concrete. Boca Raton: CRC Press LLC; 2016.

18. Greco C. Pier Luigi Nervi. Dai Primi Brevetti al Palazzo Delle Esposizioni Di Torino 1917–1948. Lucerna: Lucerne Quart Edizioni; 2008.

19. Lenticchia E, Ceravolo R, Faccio P. Understanding the structures of Pier Luigi Nervi: a multidisciplinary approach. Vitruvio. 2023;8:66–75. https://doi.org/10.4995/vitruvioijats.2023.18862

20. Mansur MA, Maalej M, Ismail M. Study on corrosion durability of ferrocement. ACI Mater J. 2008;105(1):28–34. https://doi.org/10.14359/19204

21. Masood A, Arif M, Akhtar S, Haquie M. Performance of ferrocement panels in different environments. Cem Concr Res. 2003;33(4):555–62. https://doi.org/10.1016/S0008-8846(02)01003-7

22. Nivate S, Makwana M, Kulkarni M. A study on durability parameters of ferrocement. E3S Web Conf. 2023;405:04034. https://doi.org/10.1051/e3sconf/202340504034

23. Sneha SS, Soman K, Prajith C, Davis AK, Dhanya BS. Study of the mechanical and corrosion resistance properties of ferrocement. IOP Conf Ser Earth Environ Sci. 2020;491:012033. https://doi.org/10.1088/1755-1315/491/1/012033

24. Nervi PL. Perfezionamento nella costruzione delle solette, lastre e altre strutture cementizie armate. 1944. IT 429331 (Issued September 29, 1944).

25. Nervi PL. La Struttura Portante Del Nuovo Salone Del Palazzo Di Torino Esposizioni. 1950. Rassegna Tecnica Della Società Degli Ingegneri e Architetti in Torino.

26. Nervi PL. Procedimento costruttivo per la realizzazione di strutture cementizie ondulate o curve con o senza tensione preventiva. 1948. IT 445781 (Issued August 26, 1948).

27. Nervi PL. Procedimento di costruzione per la realizzazione di superfici resistenti piane o curve costituite da reticolati di nervature in cemento armato, completate o meno da solette di collegamento tra le nervature. 1950. IT 465636 (Issued May 19, 1950).

28. Nervi PL. Costruire Correttamente. Caratteristiche e Possibilità Delle Strutture Cementizie Armate. Milan: Hoepli; 1955.

29. Nervi PL. Aesthetics and technology in building. Cambridge: Harvard University Press; 1965. https://doi.org/10.5406/j.ctv80c9j9.11

30. Nervi PL. L'evoluzione Delle Strutture in Cemento Armato. In: Colonnetti G, editor. Scienza Delle Costruzioni. La Tecnica Delle Costruzioni: Le Pareti Sottili. Volume 3. Torino: Edizioni Scientifiche Einaudi; 1957. p. 9–60.

31. Ceravolo R, Lenticchia E, Matteini I, Sorrentino G, Tondolo F. Experimental durability analysis of historical ferrocement. RILEM Bookseries. 2024;47:788–801. https://doi.org/10.1007/978-3-031-39603-8_64

32. Ceravolo R. The Halls of Turin Exhibition Center by Pier Luigi Nervi: A Multi-Disciplinary Approach for Diagnosis and Preservation. 2023. Available from: https://www.getty.edu/foundation/initiatives/current/keeping_it_modern/report_library/turin_exhibition_center.html

33. EN ISO. EN 1015-11: methods of test for mortar for masonry - part 11: determination of flexural and compressive strength of hardened mortar. European Committee for Standardization. 2019.

34. EN ISO. EN ISO 6892-1:2019 Metallic Materials - Tensile Testing Part 1: Method of Test at Room Temperature. British Standard. 2019.

35. ASTM International. *Standard test method for corrosion potentials of uncoated reinforcing steel in concrete*. ASTM C876-15. G01.14. ASTM International. 2015.

36. D'Alessandro A, Corr DJ, Shah SP. Use of tetraethyl orthosilicate to improve durability of ferrocement. ACI Mater J. 2019; 116(6):16821. https://doi.org/10.14359/51716821

AUTHOR BIOGRAPHIES

Erica Lenticchia, Department of Structural, Geotechnical and Building Engineering (DISEG), Politecnico di Torino, Torino, Italy. Email: erica.lenticchia@polito.it.

Gerardo Sorrentino, Department of Structural, Geotechnical and Building Engineering (DISEG), Politecnico di Torino, Torino, Italy. Email: gerardo.sorrentino@polito.it.

Rosario Ceravolo, Department of Structural, Geotechnical and Building Engineering (DISEG), Politecnico di Torino, Torino, Italy. Email: rosario.ceravolo@polito.it.

Francesco Tondolo, Department of Structural, Geotechnical and Building Engineering (DISEG), Politecnico di Torino, Torino, Italy. Email: francesco.tondolo@polito.it.